Probing the sound speed of dark energy with a lunar laser interferometer

Alfredo Gurrola, Robert J. Scherrer, and Oem Trivedi
Department of Physics and Astronomy, Vanderbilt University, Nashville, Tennessee, USA

(Received 7 February 2026; accepted 2 June 2026; published 6 July 2026)

The sound speed of dark energy encodes fundamental information about the microphysics underlying cosmic acceleration, yet remains essentially unconstrained by existing observations. We demonstrate that a lunar-based laser interferometer, such as the proposed Laser Interferometer Lunar Antenna (LILA), can directly probe the sound speed of dark energy by measuring the real-time evolution of horizon-scale gravitational potentials. Operating in the ultra-low-frequency gravitational band inaccessible from Earth, LILA is sensitive to scalar metric perturbations sourced by dark energy dynamics. Using both fluid and effective field theory descriptions, we develop a complete framework linking dark energy sound speed to observable strain signatures. We construct a likelihood pipeline and Fisher forecasts, showing that LILA can either detect clustering dark energy or exclude broad classes of models with unprecedented sensitivity. This establishes lunar interferometry as a novel and powerful probe of the physics driving cosmic acceleration.

DOI: 10.1103/gpyr-9tvw

I. INTRODUCTION AND MOTIVATION

Understanding the physical origin of cosmic acceleration is one of the central challenges of modern physics. While the standard ΛCDM (cold dark matter) cosmology model successfully describes a wide range of observations, the nature of dark energy [1], which dominates the energy budget of the Universe at late times, remains unknown. This has led to a huge amount of possible nontrivial realizations for dark energy, ranging from modified gravity to quantum gravitational explanations [2–5]. Most observational constraints on dark energy focus on its background equation of state parameter w, however, vastly different physical models can share identical background evolution [6–10]. A critical discriminator is the sound speed of dark energy, c_s^2, which governs the propagation of pressure perturbations and determines whether dark energy clusters gravitationally on cosmological scales.

To understand this better, we note that dark energy is usually characterized at the background level by its equation of state parameter given by

$$w \equiv \frac{p_{\rm DE}}{\rho_{\rm DE}} \tag{1}$$

where $\rho_{\rm DE}$ and $p_{\rm DE}$ denote the dark-energy density and pressure, respectively. While the background quantity w determines how dark energy modifies the expansion history, it does not by itself specify how dark energy responds to inhomogeneities and where hence that information is encoded. It is there in the sound speed of dark energy, which determines how pressure perturbations react to density perturbations. At the perturbative level one may define the rest frame sound speed through

$$c_s^2 \equiv \left(\frac{\delta p_{\rm DE}}{\delta \rho_{\rm DE}}\right)_{\rm rf} \tag{2}$$

where the subscript rf denotes the dark energy rest frame and this quantity governs the propagation of scalar fluctuations in the dark energy sector and therefore determines whether dark energy remains nearly smooth or instead clusters gravitationally on large scales.

In canonical scalar field models one usually observes $c_s^2 = 1$, implying that dark energy remains smooth but in contrast, more general theories including coupled dark energy [11–15] and effective field theory (EFT) extensions of gravity [16–21], naturally predict $c_s^2 \ll 1$ or in some cases like k essence and other noncanonical theories [22–36], $c_s^2 > 1$ too. Measuring or constraining this quantity therefore provides a direct window into the microphysics of cosmic acceleration. However, it has proven to be notoriously difficult to think of consistent ways to constrain this otherwise important quantity. To emphasize just how important this can be for dark energy model building, we note that constraints ruling $c_s^2 \sim 1$ would provide a strong robust support for a large class of canonical dark energy models, while alienating noncanonical models (except those which are finely tuned) and any notions of dark energy clustering. On the contrary, sound speeds closer to zero would signal strong clustering properties and would have revealing consequences for both canonical and noncanonical model space. On the other hand, if one observes sound speeds to be superluminal then it would provide the strongest evidence of beyond standard model and quantum gravitational physics in cosmology, as most

 © 2026 American Physical Society

noncanonical scenarios find their motivations in field theories in these regimes.

It is hence quite unfortunate that existing probes constrain c_s^2 only weakly, primarily through integrated effects such as the late-time integrated Sachs-Wolfe effect [37–43]. In this work, we propose a qualitatively new approach, which is concerned with directly measuring the real-time evolution of large scale gravitational potentials using a lunar laser interferometer such as Laser Interferometer Lunar Antenna (LILA) [44]. We show how such measurements can naturally feed into those for sound speeds for dark energy and, argue how a lunar based interferometer like LILA can provide the perfect setup for such finding such novel constraints.

II. DARK ENERGY PERTURBATIONS AND SOUND SPEED

Describing dark energy as a general fluid characterized at the background level by an equation of state parameter $w = p_{\rm DE}/\rho_{\rm DE}$ and at the perturbative level, by a rest frame sound speed c_s^2 that governs the response of pressure perturbations to density fluctuations, we start by considering linear scalar perturbations in an expanding Friedmann-Lemaitre-Robertson-Walker universe. Thereby in the Newtonian gauge the perturbed metric may be written as

$$ds^2 = -(1+2\Phi)dt^2 + a^2(t)(1-2\Psi)d\vec{x}^2 \tag{3}$$

where Φ and Ψ are the scalar gravitational potentials. For a generic fluid component, perturbation evolution is governed by the continuity and Euler equations and after combining them one finds a schematic second order equation for the dark energy density contrast $\delta_{\rm DE} = \delta\rho_{\rm DE}/\rho_{\rm DE}$. This second order differential equation is of the form

$$\ddot{\delta}_{\rm DE} + (1-3w)H\dot{\delta}_{\rm DE} + \left(\frac{c_s^2k^2}{a^2} - 4\pi G\rho\right)\delta_{\rm DE} = S(k,t) \tag{4}$$

where we note that the overdots denote derivatives with respect to cosmic time, k is the comoving wave number, and $S(k,t)$ represents source terms arising from metric perturbations and couplings to other components. The term proportional to $c_s^2k^2/a^2$ encodes the effect of pressure gradients, while the term proportional to the background density reflects gravitational instability.

The competition between these two contributions defines a characteristic scale at which pressure support balances gravitational attraction and this scale is conveniently expressed in terms of a Jeans wave number

$$k_J \sim \frac{aH}{c_s}, \tag{5}$$

which separates regimes of qualitatively different behavior [45–47]. This is to say that for modes with $k \gg k_J$, pressure gradients dominate and dark energy perturbations are strongly suppressed, causing dark energy to remain effectively smooth while for modes with $k \lesssim k_J$, pressure support is inefficient and dark energy can cluster gravitationally. In particular, when c_s^2 is sufficiently small the Jeans scale is pushed to horizon-sized wavelengths, allowing dark energy perturbations to persist and evolve on the largest observable scales at late times.

The impact of these perturbations is most clearly understood by examining the evolution of the scalar gravitational potentials as in the Newtonian gauge, the perturbed line element is written as

$$ds^2 = a^2(\tau)[-(1+2\Phi)d\tau^2 + (1-2\Psi)d\vec{x}^2] \tag{6}$$

where Φ and Ψ encode the scalar metric fluctuations. Now, if the sound speed is close to unity, $\delta\rho_{\rm DE}$ is suppressed on subhorizon scales and the late-time evolution of Φ is dominated by the dilution of matter perturbations. This ends up leading to the familiar decay of gravitational potentials during cosmic acceleration and by contrast, when c_s^2 is small enough for dark energy to cluster on horizon scales, $\delta\rho_{\rm DE}$ remains dynamically relevant and alters both the amplitude and time dependence of Φ and Ψ. This modification is not an integrated effect accumulated along a line of sight, but represents a genuine change in the real-time evolution of the metric potentials.

As these changes occur precisely on scales comparable to the Hubble radius, they are difficult to access with conventional large scale structure or CMB observables but a lunar laser interferometer, however, is sensitive to ultralow frequency fluctuations corresponding to these horizon-scale modes. This can therefore directly track the temporal behavior of Φ in the time domain and so, this capability would allow for a facility like LILA to probe the clustering properties of dark energy and to distinguish between smooth and clustering regimes by observing the dynamical imprint of c_s^2 on the evolution of scalar gravitational potentials.

III. LUNAR LASER INTERFEROMETRY AS A COSMOLOGICAL OBSERVATORY

A laser interferometer deployed on the lunar surface operates in an exceptionally quiet environment, free from atmospheric fluctuations and with significantly reduced seismic noise relative to terrestrial detectors [44]. This unique setting motivates the possibility of probing ultra-low-frequency signals. In the present work, we consider a science-driven sensitivity window

$$f \sim 10^{-7}\text{–}10^{-3}\ \text{Hz}, \tag{7}$$

corresponding to horizon-scale and near-horizon cosmological perturbations. This frequency range is selected based on the underlying physics: dark energy clustering affects metric fluctuations most strongly on scales comparable to

the Hubble radius, and therefore imprints signatures in the ultra-low-frequency regime.

We emphasize that the detailed detector configuration of a lunar laser interferometer remains in a very early conceptual stage, and no final experimental design has yet been established. As in early-stage forecasts for experiments such as laser interferometer space antenna (LISA), CMB-S4, and pulsar timing arrays, our goal is to establish the *scientific case and potential reach* under well-motivated physical assumptions, rather than to present a finalized engineering proposal. In this sense, the frequency range considered here should be interpreted as a physics-motivated target that can inform future lunar detector optimization.

Reference [44] by contrast, presents an early LILA concept optimized for a different science case, focusing on the intermediate-frequency band ($\sim 10^{-1}$ Hz) relevant for astrophysical gravitational-wave sources. These two frequency ranges probe distinct physical regimes and are therefore complementary rather than contradictory. The fact that Ref. [44] emphasizes the intermediate-frequency band does not preclude the possibility that a lunar-based interferometer could be configured to access the low-frequency regime relevant for cosmological applications. Indeed, the ultra-low-frequency window considered here lies between pulsar timing array and space-based interferometer sensitivities, and remains unexplored by existing gravitational-wave experiments.

In the presence of scalar metric perturbations, the spacetime line element in Newtonian gauge is characterized by the gravitational potential Φ, whose temporal and spatial variations induce differential phase shifts across a finite interferometer baseline. For sufficiently long baselines and low frequencies, these scalar induced distortions then manifest as an effective strain,

$$h_{\rm eff}(t) \simeq \frac{\Delta\Phi(t)}{c^2} \tag{8}$$

where $\Delta\Phi(t)$ denotes the potential difference sampled by the interferometer arms. Interestingly, unlike tensor gravitational waves, this signal reflects the real-time evolution of large scale gravitational potentials rather than propagating wave solutions. The statistical properties of the measured strain are therefore directly related to those of the scalar potential, and in the frequency domain the strain power spectrum can be expressed as

$$P_h(f) \propto P_\Phi(k)|_{k\approx 2\pi f/c}. \tag{9}$$

This ends up establishing a direct correspondence between ultra-low-frequency strain fluctuations and the power spectrum of gravitational potentials at horizon-scale wave numbers.The physical significance of this correspondence lies in the dynamical equation governing Φ as on large scales and at late times, the generalized Poisson and evolution equations for the Newtonian potential receive contributions not only from matter density perturbations but also from dark energy perturbations too. One may write

$$k^2\Phi + 3a^2H(\dot{\Phi} + H\Phi) \propto a^2(\delta\rho_m + \delta\rho_{\rm DE}) \tag{10}$$

where $\delta\rho_{\rm DE}$ denotes fluctuations in the dark energy component and the amplitude and time dependence of $\delta\rho_{\rm DE}$ are controlled by the microphysical properties of dark energy, most notably its effective sound speed, which determines whether pressure gradients suppress or allow clustering on horizon scales.

This is crucial because if the sound speed is close to unity, dark energy perturbations remain smooth on sub-horizon scales and contribute negligibly to the right-hand side of the above equation which would end up leading to the standard late time decay of Φ. In contrast, for sufficiently small sound speed we see that pressure support is weak and dark energy clusters alongside matter on large scales, sourcing the gravitational potential and modifying both its amplitude and temporal evolution. These modifications translate directly into excess low-frequency power and altered time domain correlations in $P_\Phi(k)$, and hence in the measured strain spectrum $P_h(f)$. LILA is therefore sensitive to the sound speed of dark energy not by directly probing its equation of motion, but by measuring the imprint of dark energy perturbations on horizon scale gravitational potentials. By resolving the frequency dependence and temporal coherence of scalar induced strain in the ultra-low-frequency band, one sees that LILA effectively constrains whether dark energy behaves as a smooth background component or as a clustering fluid. This would allow us to provide a direct observational handle on its perturbative microphysics that is complementary to background expansion probes.

While existing observatories such as LIGO-VIRGO-KAGRA (LVK), LISA and pulsar timing arrays like NANOGrav can probe complementary frequency bands, they are not optimized for continuous, coherent measurements of scalar induced metric fluctuations on horizon scales. Ground based detectors like LVK operate at much higher frequencies ($\gtrsim$10 Hz), while LISA targets milli-Hz bands dominated by compact binary sources, and pulsar timing arrays rely on integrated timing residuals rather than direct, time-resolved strain measurements. In contrast, a LILA setup would offer a uniquely quiet and stable environment that can, in principle access ultra-low frequency, long wavelength scalar perturbations in a direct and continuous manner. It would hence end up enabling sensitivity to the real time evolution of gravitational potentials relevant for dark energy clustering.

IV. EFFECTIVE FIELD THEORY OF DARK ENERGY

A model-independent description of dark energy dynamics is provided by the EFT of cosmic acceleration [16]. In unitary gauge, the action is

$$S = \int \left[\frac{M_*^2}{2} R - \Lambda(t) - c(t) g^{00} + \frac{M_2^4(t)}{2} (\delta g^{00})^2 + \cdots \right] d^4x \sqrt{-g}. \tag{11}$$

The sound speed of scalar perturbations is given by

$$c_s^2 = \frac{c(t)}{c(t) + 2M_2^4(t)}. \tag{12}$$

LILA constrains c_s^2 by directly measuring scalar-metric mixing through time-dependent strain. This enables constraints on EFT operators that are otherwise unconstrained by background cosmology or large-scale structure. We can discuss a more general construction here by extending the effective field theory action beyond the minimal truncation considered above. In full generality, the EFT of dark energy in unitary gauge admits additional operators consistent with time-dependent spatial diffeomorphism invariance, including couplings between the lapse, extrinsic curvature, and spatial curvature. A representative extension of the action takes the schematic form

$$S = \int d^4x \sqrt{-g} \left[\frac{M_*^2(t)}{2} R - \Lambda(t) - c(t) g^{00} + \frac{M_2^4(t)}{2} (\delta g^{00})^2 - \frac{m_3^3(t)}{2} \delta g^{00} \delta K + \mu_2^2(t) (\delta K^2 - \delta K_{ij} \delta K^{ij}) + \cdots \right] \tag{13}$$

where we note that the ellipsis denotes higher-order operators in fluctuations or operators involving higher spatial derivatives. While these terms do not affect the homogeneous background evolution at leading order, they play an essential role in shaping the dynamics of scalar perturbations. Restoring time diffeomorphism invariance through the Stückelberg field π, defined via $t \to t + \pi(x^\mu)$, we can then expand the action to quadratic order in scalar perturbations. This would give us an effective action for the single propagating scalar degree of freedom after integrating out the nondynamical lapse and shift variables. The resulting quadratic action can always be cast in the form

$$S^{(2)} = \int dt\, d^3x\, a^3 \left[A_{\rm eff}(t) \dot{\zeta}^2 - \frac{B_{\rm eff}(t)}{a^2} (\nabla \zeta)^2 \right] \tag{14}$$

where ζ denotes the gauge-invariant curvature perturbation. The functions $A_{\rm eff}$ and $B_{\rm eff}$ depend on the full set of EFT coefficients, the background expansion rate, and the matter content. In this general setting, the squared sound speed of dark energy perturbations is defined invariantly as

$$c_s^2 = \frac{B_{\rm eff}(t)}{A_{\rm eff}(t)}. \tag{15}$$

This expression makes clear that the sound speed is not a fundamental parameter but an emergent quantity encoding the relative strength of spatial gradient terms to temporal kinetic terms in the scalar sector. Operators such as $(\delta g^{00})^2$ primarily enhance $A_{\rm eff}$ by increasing the inertia of scalar fluctuations, while braiding type operators proportional to $\delta g^{00} \delta K$ and extrinsic-curvature combinations can modify both $A_{\rm eff}$ and $B_{\rm eff}$ through kinetic mixing with the metric. The simple expression for c_s^2 obtained earlier (12) is recovered when the dominant modification to the scalar sector arises from the $(\delta g^{00})^2$ operator and when mixing with metric perturbations is subleading in the decoupling limit and this situation is typical in scenarios where braiding and higher derivative operators are either absent or constrained independently by gravitational wave and large scale structure observations. In such cases, the minimal form provides an accurate and transparent parametrization for forecasting and data analysis. The more general form only becomes relevant when kinetic mixing between the scalar and the metric is significant or when higher order curvature operators contribute comparably to the quadratic action.

From the perspective of observational constraints, measurements that probe horizon scale potential evolution are primarily sensitive to the effective sound speed itself rather than to the detailed operator decomposition of $A_{\rm eff}$ and $B_{\rm eff}$. So in that sense, constraints obtained under the minimal parametrization can be interpreted as constraints on the effective propagation speed of scalar perturbations, remaining robust across a broad class of EFT realizations. Only in scenarios where multiple operators conspire to produce rapidly evolving $A_{\rm eff}$ and $B_{\rm eff}$ would a fully general treatment be required to accurately interpret the data.

V. MOCK STRAIN POWER SPECTRA

A key element of this work is the construction of a mock strain power spectrum for a lunar laser interferometer that is physically grounded in cosmological scalar perturbations. In this Section we describe the mock spectrum derived from a fiducial ΛCDM cosmology characterized by $\Omega_m = 0.3$, $\Omega_{\rm DE} = 0.7$, and $w = -1$ using linear perturbation theory.

We first describe the derivation of the transfer function governing the evolution of the Newtonian potential in the presence of a dark energy component with nontrivial sound speed. This derivation connects the asymptotic solutions of the scalar perturbation equation to the phenomenological transfer function which can be computed numerically (e.g., using CLASS or CAMB) and is employed in the construction of mock strain spectra for lunar laser interferometry.

We consider the evolution of Φ in the presence of a dark energy fluid with sound speed c_s^2. Working in conformal time τ and Newtonian gauge, the evolution equation derived from Einstein's equations and energy-momentum conservation is a second-order linear ordinary differential equation whose solution is fully determined by initial conditions and the background expansion. As noted previously, the key physical scale governing the behavior of solutions is the sound horizon (also known as the Jeans wave number), $k_J(\tau) \equiv \frac{aH}{c_s}$, which separates modes that are pressure supported from those that are not. The qualitative behavior of Φ depends on whether a given Fourier mode satisfies $k \ll k_J$ or $k \gg k_J$. For modes well outside the sound horizon, the pressure term can be neglected, i.e., $c_s^2 k^2 \ll \frac{a'}{a}\partial_\tau$, and the Einstein field equations give rise to a solution of the form

$$\Phi(\tau) = C_1 + C_2 \int d\tau\, a^{-(2+3c_s^2)}, \tag{16}$$

where $C_{1,2}$ are determined by the early and late time boundary conditions. At late times the second term decays, leaving

$$\Phi(k,\tau) \xrightarrow{k \ll k_J} \Phi_{\rm prim}(k). \tag{17}$$

Therefore, modes larger than the sound horizon characterized by k_J retain their primordial amplitude. For modes deep inside the sound horizon, the gradient term dominates, i.e., $c_s^2 k^2 \gg \frac{a'}{a}\partial_\tau$, and the Einstein field equations for Φ result in solutions of the form $\Phi(\tau) = A(k)e^{ic_s k\tau} + B(k)e^{-ic_s k\tau}$. However, cosmic expansion damps the amplitude of these oscillations. Accounting for the Hubble friction term in the full equation, the envelope of the solution scales as $\Phi \propto a^{-\frac{1}{2}(2+3c_s^2)}$. Hence, for $k \gg k_J$,

$$\Phi(k,\tau) \ll \Phi_{\rm prim}(k), \tag{18}$$

with oscillatory behavior and strong suppression.

Because the Einstein field equation for Φ is linear and smooth in k, the full solution must interpolate continuously between the two asymptotic regimes described above. We can therefore write the general solution in the factorized form

$$\Phi(k,\tau) = \Phi_{\rm prim}(k) T(k/k_J), \tag{19}$$

where the function $T(k/k_J)$ satisfies $T(k/k_J \ll 1) = 1$ and $T(k/k_J \gg 1) \ll 1$. The simplest analytic function that satisfies these conditions and reproduces the correct asymptotic behavior is

$$T_\Phi(k, c_s^2) = \frac{1}{1 + (\frac{k}{k_J})^2} = \frac{1}{1 + (\frac{c_s k}{aH})^2}. \tag{20}$$

Therefore, the transfer function for the Newtonian potential contains the primordial value of the Newtonian potential $\Phi_{\rm prim}(k)$ set by inflation, and $\Phi(k,\tau)$ is its late-time value after linear evolution in an expanding universe. The transfer function thus isolates the scale-dependent effects of late-time physics from the initial conditions. This transfer function explicitly encodes the role of the dark energy sound speed. For $c_s^2 \sim 1$, pressure support suppresses clustering on horizon scales, while for $c_s^2 \ll 1$ the sound horizon moves to high k, allowing dark energy perturbations to cluster efficiently. This scale-dependent suppression is the physical origin of the sound-speed sensitivity in the strain spectra from lunar laser interferometry.

The time-dependent power spectrum of the potential is related to the transfer function and the primordial power spectrum. Since the primordial field $\Phi_{\rm prim}(k)$ is a stochastic field generated during inflation, its statistical properties are fully specified by its two-point function, and when combined with the Fourier-space correlator using the inverse Fourier transform, it leads directly to $\langle \Phi_{\rm prim}(\mathbf{k}) \Phi^*_{\rm prim}(\mathbf{k}') \rangle = (2\pi)^3 \delta^{(3)}(\mathbf{k} - \mathbf{k}') P_\Phi^{\rm prim} \times (k)$. Using $\Phi(\mathbf{k},\tau) = T_\Phi(\mathbf{k}, c_s^2)\Phi_{\rm prim}(\mathbf{k})$, we obtain $\langle \Phi(\mathbf{k},\tau)\Phi^*(\mathbf{k}',\tau)\rangle = (2\pi)^3 \delta^{(3)}_{k,k'} T_\Phi^2(\mathbf{k}, c_s^2) P_\Phi^{\rm prim}(\mathbf{k})$.

Therefore,

$$P_\Phi(k,\tau) = T_\Phi^2(k, c_s^2) P_\Phi^{\rm prim}(k). \tag{21}$$

Similarly, the statistical nature of the strain power spectrum is defined by $\langle h(\mathbf{k},\tau) h^*(\mathbf{k}',\tau)\rangle = (2\pi)^3 \delta^{(3)}_{k,k'} P_h(k,\tau)$, but after accounting for the dependence of the strain h on $\Phi(k,\tau)$, we arrive at an explicit equation for how the statistical properties of the measured strain are directly related to those of the scalar potential and in the frequency domain. The strain power spectrum can be expressed as

$$P_h(f) = T_\Phi^2(k, c_s^2) P_\Phi^{\rm prim}(k). \tag{22}$$

In constructing the mock strain power spectra $P_h(f)$, the cosmological scalar perturbations are mapped onto an effective interferometric observable through an explicit detector response function. The measured strain can be written schematically as $h(\mathbf{k}, f) = \mathcal{R}(f, \hat{\mathbf{k}})\Phi(\mathbf{k})$, where $\mathcal{R}(f, \hat{\mathbf{k}})$ encodes the geometric response of the detector, including arm orientation, baseline length, and the coherence of long-wavelength modes across the interferometer. However, since a lunar laser interferometer has not yet been constructed, the mock strain spectra necessarily adopts a simplified and conservative treatment of the detector response. This approximation is well justified for the ultra-low-frequency regime of interest, where the

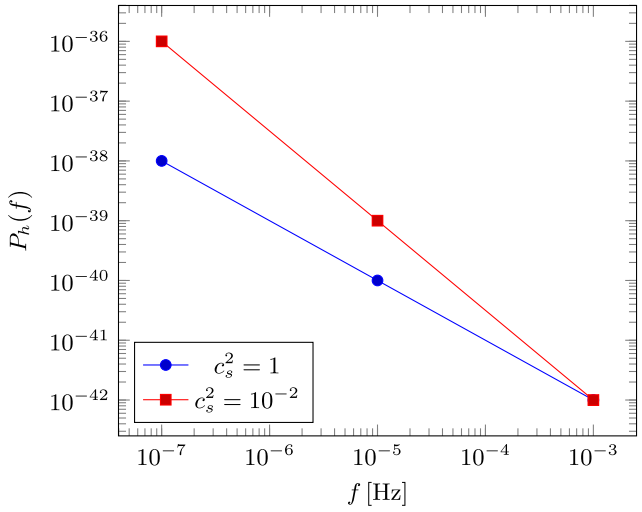

FIG. 1. Mock strain power spectra illustrating enhanced low-frequency power for clustering dark energy.

wavelengths of scalar perturbations are many orders of magnitude larger than any plausible lunar baseline, placing the experiment firmly in the long-wavelength limit. In this regime, scalar-induced tidal distortions are coherent across the interferometer, and the response becomes effectively independent of arm orientation, baseline length, and detailed geometry, up to an overall factor of order unity. Accordingly, the detector response is modeled as an isotropic, orientation-averaged transfer function that can be absorbed into an effective normalization of the strain. The resulting strain power spectrum is then given by $P_h(f) = |\mathcal{R}(f)|^2 P_\Phi(k)$, evaluated at $k = 2\pi f/c$. This approach isolates the cosmological dependence of the signal, particularly its sensitivity to the dark energy sound speed, while avoiding assumptions tied to a specific engineering implementation. More detailed response modeling can be straightforwardly incorporated once a concrete detector design is specified, but does not affect the qualitative or quantitative conclusions of this work.

For sound speeds $c_s^2 = \{1, 10^{-2}\}$, the resulting strain spectra are shown in Fig. 1 and exhibit an approximately power-law behavior over the frequency range 10^{-7}–10^{-3} Hz. This near-linear behavior on log-log axes reflects the combined scaling of the primordial spectrum and the large-scale gravitational transfer function, with decreasing c_s^2 leading to an overall enhancement of power due to increased dark energy clustering. At sufficiently high frequencies near 10^{-3} Hz, corresponding to modes well inside the dark energy sound horizon, the mock strain power spectra begin to converge and become effectively independent of the dark energy sound speed. This behavior reflects the fact that on small scales the Newtonian potential—and hence the induced interferometric strain—is dominated by matter perturbations, while dark energy fluctuations are strongly pressure supported and do not contribute appreciably. As a result, variations in the dark energy sound speed leave no observable imprint on the strain spectrum in this regime, leading to the observed convergence of all curves at high frequency. Conversely, at low frequencies near the horizon scale, dark energy perturbations can cluster if the sound speed is sufficiently small, producing order-of-magnitude differences in the strain power spectrum. This scale-dependent transition highlights the unique sensitivity of a lunar laser interferometer, which operates precisely in the ultra-low-frequency band where dark energy microphysics leaves an observable imprint, and underscores its potential to directly constrain the sound speed of dark energy in a manner inaccessible to terrestrial or space-based interferometers.

VI. LIKELIHOOD FRAMEWORK AND FORECAST METHODOLOGY

In this Section we describe the statistical framework used to assess the sensitivity of a lunar laser interferometer such as LILA to the sound speed of dark energy. We first introduce the likelihood formalism that connects theoretical predictions for the strain power spectrum to hypothetical interferometric measurements, and then describe how the Fisher information matrix is employed to generate forecasts, discovery prospects, and exclusion limits.

The fundamental observable considered in this work is the strain power spectrum, $P_h(f)$. For a given set of cosmological parameters $\boldsymbol{\theta} = \{c_s^2, w, \Omega_{\rm DE}\}$, the theory predicts a model spectrum $P_h^{\rm th}(f;\boldsymbol{\theta})$. A measurement by LILA yields an estimator $\hat{P}_h(f)$ with associated uncertainty determined by instrumental noise and finite observation time.

Assuming that the strain fluctuations are Gaussian and statistically stationary, the likelihood of observing a given $\hat{P}_h(f)$ is well approximated by a Gaussian likelihood in power-spectrum space [48–50],

$$\mathcal{L}(\boldsymbol{\theta}) \propto \exp\left[-\frac{1}{2}\sum_f \frac{[\hat{P}_h(f) - P_h^{\rm th}(f;\boldsymbol{\theta})]^2}{\sigma_h^2(f)}\right], \quad (23)$$

where $\sigma_h(f)$ denotes the variance of the strain power spectrum estimator in each frequency bin. In practice, $\sigma_h(f)$ is determined by the detector noise power spectrum and the effective number of independent measurements accumulated during the mission lifetime.

To forecast the sensitivity of LILA prior to the availability of real data, we employ the Fisher information matrix formalism [48–50]. The Fisher matrix provides a local, quadratic approximation to the likelihood around a fiducial parameter set $\boldsymbol{\theta}_0$, and quantifies the amount of information that an experiment is expected to obtain about each parameter. The Fisher matrix is defined as

$$F_{ij} \equiv -\left\langle \frac{\partial^2 \ln \mathcal{L}}{\partial\theta_i \partial\theta_j} \right\rangle = \sum_f \frac{1}{\sigma_h^2(f)} \frac{\partial P_h^{\rm th}(f)}{\partial\theta_i} \frac{\partial P_h^{\rm th}(f)}{\partial\theta_j}, \quad (24)$$

where the derivatives are evaluated at the fiducial cosmology. In this work, the parameter set includes the dark energy sound speed c_s^2 and w, while the other background cosmological parameters are fixed to their ΛCDM values unless stated otherwise. The inverse Fisher matrix approximates the covariance of the parameters,

$$\mathrm{Cov}(\theta_i, \theta_j) \simeq (F^{-1})_{ij}, \quad (25)$$

so that the marginalized 1σ uncertainty on a parameter θ_i is given by $\sigma(\theta_i) = \sqrt{(F^{-1})_{ii}}$.

Within this framework, the Fisher matrix serves three closely related purposes. First, it provides forecasts for the expected precision with which LILA can measure or constrain the dark energy sound speed, assuming a given fiducial value. Second, it allows us to assess discovery prospects by determining whether deviations from the canonical value $c_s^2 = 1$ would produce a statistically significant change in the strain spectrum relative to the experimental uncertainties. Finally, the Fisher formalism enables exclusion statements by identifying regions of parameter space for which the predicted strain signal would be inconsistent with a null or reference model at a specified confidence level.

The Fisher forecasts presented in this work are based on an idealized but physically well-motivated treatment of statistical uncertainties. In the absence of a finalized instrumental design for a lunar laser interferometer, we do not assume a specific noise power spectrum, arm configuration, or mission lifetime. Instead, we adopt a conservative signal-dominated approximation in the ultra-low-frequency regime of interest, where scalar-induced strain fluctuations are coherent across the detector and cosmic variance provides a natural lower bound on achievable uncertainties.

To provide a concrete point of reference, we note that one proposed configuration discussed in Ref. [44], often referred to as "LILA Horizon," consists of a ∼40 km triangular interferometer with a combination of suspended and unsuspended optical elements, operating near ambient lunar temperatures (∼300 K). In such a configuration, and in the absence of significant seismic contamination, the dominant low-frequency noise source is expected to arise from thermal noise in the optics and coatings. Adopting a representative displacement noise power spectral density comparable, at the level of order-of-magnitude estimates, to that of optical coatings in current ground-based interferometers, $S_x^{\rm thermal}(f) \sim 10^{-33}\ \mathrm{m^2/Hz}(f/\mathrm{Hz})^{-1}$, this translates into a strain noise level $h_{\rm thermal}(f) \sim \sqrt{f S_x^{\rm thermal}(f)}/L \sim 10^{-22}$ for a characteristic baseline $L \sim 40$ km across the frequency interval $f \sim 10^{-7}$–10^{-3} Hz, up to order-unity factors.

In addition, advances in calibration and analysis techniques in gravitational-wave experiments, including the use of machine learning methods, have demonstrated the ability to control and calibrate strain measurements at the $\mathcal{O}(1\%)$ [51]. While a direct extrapolation to lunar interferometry requires caution, this suggests that subdominant signals ($\mathcal{O}(1\%) \times h_{\rm thermal} \sim 10^{-24}$) below the nominal noise level may be accessible with sufficient integration time and robust analysis pipelines.

For comparison, the scalar-induced strain signal in our benchmark models is characterized by a power spectrum $P_h(f) \sim 10^{-38}$–10^{-42}, corresponding to a characteristic strain $h_{\rm DE}(f) = \sqrt{f P_h(f)} \sim 10^{-20}$–$10^{-22}$, depending on frequency and sound speed. At the level of these estimates, the expected dark energy signal is comparable to or larger than the projected thermal noise floor for a lunar interferometer with parameters similar to the "LILA Horizon" configuration. This suggests that the signal lies within the range of potentially detectable strain amplitudes in the ultra-low-frequency regime considered in this work, thereby supporting the validity of the signal-dominated approximation adopted in our Fisher forecasts.

The variance of the strain power spectrum estimator is modeled using the standard Gaussian expression, with the effective number of modes per frequency bin absorbed into an overall normalization. This approach isolates the fundamental information content of the signal and yields design-agnostic forecasts for the sensitivity of LILA to the dark energy sound speed. The methodology is identical in spirit to that employed in early sensitivity forecasts for space-based interferometers [52,53], predesign pulsar timing array cosmology studies [54–56], CMB-S4 delensing projections [57–59], and 21-cm dark ages proposals [60,61], where the primary goal is to establish the underlying scientific reach prior to detailed engineering optimization. More comprehensive noise modeling and mission-specific performance estimates can be straightforwardly incorporated once a concrete detector architecture is specified, but are not required to assess the qualitative or quantitative conclusions of this study.

VII. FORECASTS, DISCOVERY, AND EXCLUSION

Figures 2 and 3 show the illustrative Fisher contour ellipses in the (w, c_s^2) plane centered on the fiducial model $(w, c_s^2) = (-1, 10^{-2})$ and $(w, c_s^2) = (-1, 10^{-3})$, including the 2σ, 3σ, and 5σ joint confidence regions. The elongated shape of the contours reflects a partial degeneracy between the dark energy equation of state and the sound speed, arising from the fact that variations in w primarily affect the background expansion history, while c_s^2 controls the scale-dependent clustering of dark energy through the sound horizon. The narrow extent of the contours along the c_s^2

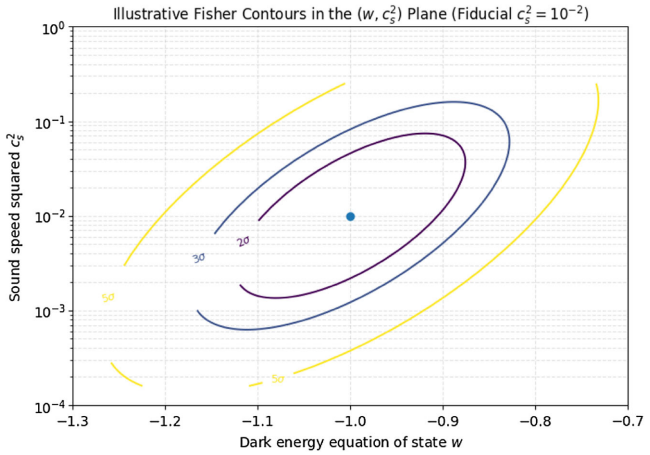

FIG. 2. Fisher contour ellipses in the (w, c_s^2) plane for a lunar laser interferometer, centered on the fiducial clustering dark energy model $(w, c_s^2) = (-1, 10^{-2})$. Shown are the joint 2σ, 3σ, and 5σ confidence regions obtained using the cosmology-calibrated mock strain power spectrum.

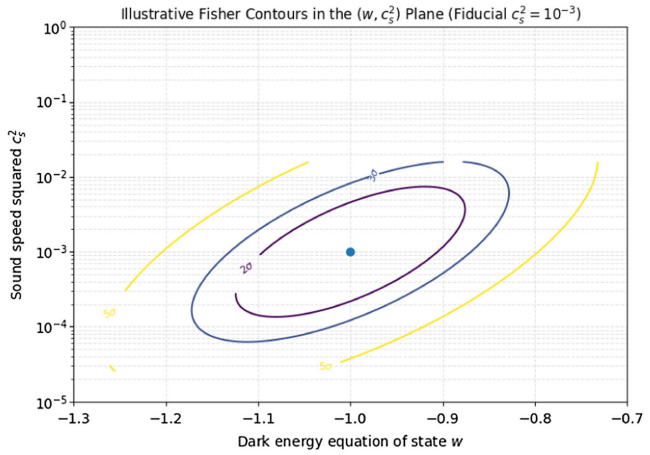

FIG. 3. Fisher contour ellipses in the (w, c_s^2) plane for a lunar laser interferometer, centered on the fiducial clustering dark energy model $(w, c_s^2) = (-1, 10^{-3})$. Shown are the joint 2σ, 3σ, and 5σ confidence regions obtained using the cosmology-calibrated mock strain power spectrum.

direction demonstrates that the strain power spectrum measured by a lunar laser interferometer is highly sensitive to the sound speed, particularly in the ultra-low-frequency regime where dark energy perturbations contribute significantly to the gravitational potential.

The Fisher contour analysis is updated in Figs. 3–5 to include a Gaussian prior constraining the dark energy equation-of-state parameter to lie within 3% uncertainty of $w = -1$, reflecting one of the tightest widely quoted bounds from a single coherent global analysis in the final *Planck* 2018 cosmological-parameters results when combined with baryon acoustic oscillations and Type Ia supernovae [62]. Incorporating this external information

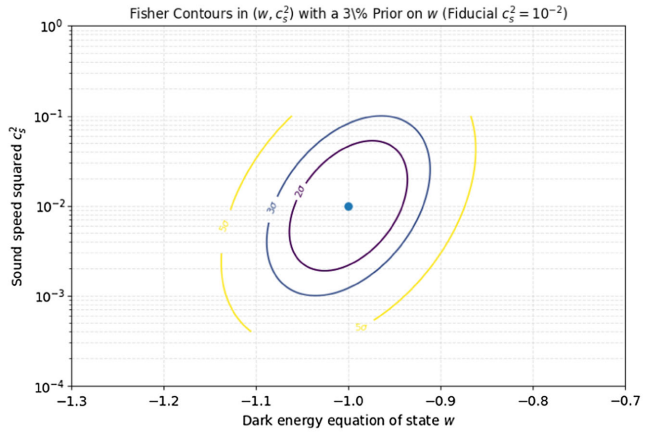

FIG. 4. Fisher contour ellipses in the (w, c_s^2) plane for a lunar laser interferometer, centered on the fiducial clustering dark energy model $(w, c_s^2) = (-1, 10^{-2})$ with w constrained within 3% of -1 using a Gaussian prior. Shown are the joint 2σ, 3σ, and 5σ confidence regions obtained using the cosmology-calibrated mock strain power spectrum.

significantly tightens the contours in the w direction and correspondingly reduces the degeneracy-induced broadening of the sound-speed constraint, since restricting the allowed variation in w limits the extent to which background expansion effects can mimic the scale-dependent spectral turnover induced by a finite dark energy sound speed. When viewed over a wider range in w, the contours are seen to occupy only a small region around ΛCDM, making clear that the remaining uncertainty budget is dominated by c_s^2. This demonstrates that the inferred constraint on the dark energy sound speed is not driven by residual freedom in the background expansion history, but instead arises from genuine sensitivity to dark energy perturbation physics encoded in the ultra-low-frequency strain spectrum.

The presence of well-separated 3σ and 5σ contours indicates that models with $c_s^2 \ll 1$ can be robustly distinguished from the canonical smooth dark energy case $c_s^2 = 1$, even after marginalizing over w. In particular, the exclusion of $c_s^2 = 1$ at high statistical significance for a fiducial clustering model provides strong evidence that LILA has discovery-level sensitivity to dark energy microphysics, enabling a qualitative test of whether dark energy clusters on cosmological scales rather than merely tightening constraints on its background equation of state.

This framing aligns with discovery thresholds used in high-impact cosmology experiments. Another subtlety that one should keep in mind while discussing possible sound speed constraints is how this relates to constraints on the equation of state of dark energy. Constraints on the dark energy EOS parameter are commonly parametrized in terms of $w(a) = w_0 + w_a(1 - a)$ or equivalent forms and they arise entirely from the background expansion history of the universe. Observables such as supernova luminosity

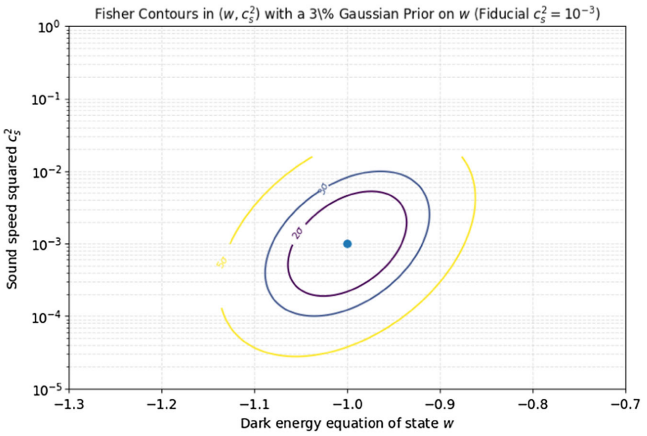

FIG. 5. Fisher contour ellipses in the (w, c_s^2) plane for a lunar laser interferometer, centered on the fiducial clustering dark energy model $(w, c_s^2) = (-1, 10^{-3})$ with w constrained within 3% of -1 using a Gaussian prior. Shown are the joint 2σ, 3σ, and 5σ confidence regions obtained using the cosmology-calibrated mock strain power spectrum.

distances, baryon acoustic oscillations and the cosmic microwave background primarily constrain the Hubble rate $H(a)$ and integrated distance measures, which depend only on the homogeneous dark energy density and pressure. At this level it should be noted that dark energy is characterized solely by its background stress-energy tensor and perturbative properties do not enter. Within the EFT framework, the background evolution is governed by the time dependent functions $\Lambda(t)$ and $c(t)$ appearing in the action and these functions determine the dark energy density and pressure through

$$\rho_{\rm DE} = \Lambda + c, \tag{26}$$

$$p_{\rm DE} = -\Lambda + c \tag{27}$$

leading to

$$w(a) = \frac{p_{\rm DE}}{\rho_{\rm DE}} = \frac{c - \Lambda}{c + \Lambda}. \tag{28}$$

As a result, observational constraints on w_0 and w_a translate directly into constraints on the background combinations of $\Lambda(t)$ and $c(t)$, fixing how the dark energy density evolves with time but leaving other EFT coefficients unconstrained.

On the other hand, the squared sound speed c_s^2 remains a property of the perturbation sector and depends on the structure of the quadratic action for scalar fluctuations and even in the minimal EFT truncation, the sound speed is given by (12), where the coefficient $M_2^4(t)$ multiplies an operator that vanishes identically on the homogeneous background. In this case, $M_2^4(t)$ has no impact on the background expansion and is therefore invisible to probes that constrain $w(a)$ and this separation persists in the more general case, where c_s^2 is determined by the ratio $B_{\rm eff}/A_{\rm eff}$ and depends on EFT operators that do not affect the background equations of motion. This structural separation implies that even extremely tight bounds on w_0 and w_a, including results consistent with $w = -1$ at subpercent level, do not in themselves restrict the sound speed of dark energy. Models with identical background evolution and identical $w(a)$ can exhibit widely different clustering behavior depending on the values of perturbation-sector coefficients and in particular, scenarios with $w(a) \simeq -1$ can support sound speeds ranging from order unity to values far below unity without violating any background constraints.

The measurements discussed here therefore probe an orthogonal direction in theory space compared to traditional dark energy surveys. While background observables determine how dark energy redshifts, constraints on c_s^2 determine how dark energy responds to inhomogeneities and whether it clusters on horizon scales and thus, combining both types of measurements allows one to disentangle background dynamics from microphysical properties. This would allow us to break degeneracies that cannot be resolved using $w_0 w_a$ constraints alone and provide a more complete characterization of the dark energy sector.

VIII. CONCLUSIONS

We have demonstrated that a lunar laser interferometer enables a qualitatively new probe of dark energy microphysics. By measuring horizon-scale gravitational potential evolution in real time, LILA directly constrains the sound speed of dark energy and associated EFT operators.

It is worth emphasizing that the constraints discussed here do not rely on dark energy being locally coupled to matter or remaining unscreened in high density environments. The observable targeted by a lunar laser interferometer is the time dependent evolution of scalar gravitational potentials on horizon scales which are governed by the gravitational contribution of dark energy perturbations and remains present even in theories where local fifth forces are efficiently screened. As a result, we see that the inferred constraints on the effective sound speed probe the clustering and propagation properties of dark energy at cosmological scales, and this is independent of local coupling or screening assumptions. While specific model interpretations may depend on how screening operates away from the linear regime, the core result that LILA constrains whether dark energy behaves as a smooth or clustering component, applies broadly across dark energy scenarios consistent with linear cosmological perturbation theory.

Building on the last point that the constraints discussed here cannot be termed simply as local, it is important to clarify what is meant by the clustering of dark energy and how this notion connects to cosmological observables. In this context, clustering does not refer to the formation of

localized overdense structures analogous to matter halos, but rather to the ability of dark energy perturbations to remain dynamically relevant on large, near horizon scales. The sound speed controls whether pressure gradients efficiently erase these perturbations or allow them to persist and contribute to the gravitational potentials. When $c_s^2 \ll 1$, the associated sound horizon approaches the Hubble scale, which thus ends up enabling dark energy fluctuations to coherently modify the evolution of Φ and Ψ across cosmological distances. These modifications are not confined to any particular region of space, but instead reflect a global change in the evolution of metric perturbations that is encoded in the large scale structure of spacetime itself. Consequently, the notion of clustering probed here is intrinsically tied to the behavior of dark energy within the framework of linear cosmological perturbation theory and this directly connects to the same physics governing the growth of structure, the evolution of gravitational potentials, and other horizon scale observables in standard cosmology.

This work aims to establish the cosmological information content and characteristic spectral imprint of dark energy perturbations accessible to a lunar laser interferometer, rather than to present a finalized instrumental noise or systematics model. In the absence of a realized detector, the analysis relies on strain spectra constructed using a treatment of the detector response, which follows the standard methodology of early sensitivity forecasts for related cosmological probes. While more detailed noise modeling and mission-specific performance estimates can be incorporated once a concrete detector architecture is specified, such refinements are not required to support the qualitative or quantitative conclusions of this study.

This approach is novel, complementary to existing probes, and capable of either discovering dark energy clustering or excluding large classes of theoretical models. Our results establish lunar interferometry as a transformative tool in the study of cosmic acceleration.

ACKNOWLEDGMENTS

We gratefully acknowledge support from Vanderbilt University and the U.S. National Science Foundation. This work is supported in part by NSF Award No. PHY-2411502 and by the Vanderbilt Discovery Doctoral Fellowship.

DATA AVAILABILITY

There are no publicly available research data or software supporting this manuscript. Requests for further information or data should be sent to the authors.

[1] A. G. Riess *et al.* (Supernova Search Team), Observational evidence from supernovae for an accelerating universe and a cosmological constant, Astron. J. **116**, 1009 (1998).
[2] M. Li, X.-D. Li, S. Wang, and Y. Wang, Dark energy: A brief review, Front. Phys. (Beijing) **8**, 828 (2013).
[3] M. Li, X.-D. Li, S. Wang, and Y. Wang, Dark energy, Commun. Theor. Phys. **56**, 525 (2011).
[4] M. J. Mortonson, D. H. Weinberg, and M. White, Dark energy: A short review, arXiv:1401.0046.
[5] D. Huterer and D. L. Shafer, Dark energy two decades after: Observables, probes, consistency tests, Rep. Prog. Phys. **81**, 016901 (2018).
[6] S. Vagnozzi, L. Visinelli, P. Brax, A.-C. Davis, and J. Sakstein, Direct detection of dark energy: The XENON1T excess and future prospects, Phys. Rev. D **104**, 063023 (2021).
[7] S. A. Adil, U. Mukhopadhyay, A. A. Sen, and S. Vagnozzi, Dark energy in light of the early JWST observations: case for a negative cosmological constant?, J. Cosmol. Astropart. Phys. 10 (2023) 072.
[8] E. Di Valentino, S. Gariazzo, O. Mena, and S. Vagnozzi, Soundness of dark energy properties, J. Cosmol. Astropart. Phys. 07 (2020) 045.
[9] S. Nojiri and S. D. Odintsov, Unified cosmic history in modified gravity: From F(R) theory to Lorentz non-invariant models, Phys. Rep. **505**, 59 (2011).
[10] S. Nojiri and S. D. Odintsov, Introduction to modified gravity and gravitational alternative for dark energy, Int. J. Geom. Methods Mod. Phys. **4**, 115 (2007).
[11] B. Gumjudpai, T. Naskar, M. Sami, and S. Tsujikawa, Coupled dark energy: Towards a general description of the dynamics, J. Cosmol. Astropart. Phys. 06 (2005) 007.
[12] A. Gómez-Valent, V. Pettorino, and L. Amendola, Update on coupled dark energy and the H_0 tension, Phys. Rev. D **101**, 123513 (2020).
[13] B. J. Barros, Kinetically coupled dark energy, Phys. Rev. D **99**, 064051 (2019).
[14] J.-Q. Xia, Constraint on coupled dark energy models from observations, Phys. Rev. D **80**, 103514 (2009).
[15] A. V. Macciò, C. Quercellini, R. Mainini, L. Amendola, and S. A. Bonometto, Coupled dark energy: Parameter constraints from n-body simulations, Phys. Rev. D **69**, 123516 (2004).
[16] N. Frusciante and L. Perenon, Effective field theory of dark energy: A review, Phys. Rep. **857**, 1 (2020).
[17] G. Gubitosi, F. Piazza, and F. Vernizzi, The effective field theory of dark energy, J. Cosmol. Astropart. Phys. 02 (2013) 032.
[18] E. V. Linder, G. Sengör, and S. Watson, Is the effective field theory of dark energy effective?, J. Cosmol. Astropart. Phys. 05 (2016) 053.

[19] J. Bloomfield, É. É. Flanagan, M. Park, and S. Watson, Dark energy or modified gravity? An effective field theory approach, J. Cosmol. Astropart. Phys. 08 (2013) 010.
[20] J.-H. Liang, Y. Liao, X.-D. Ma, and H.-L. Wang, Dark sector effective field theory, J. High Energy Phys. 12 (2023) 172..
[21] N. Frusciante, M. Raveri, and A. Silvestri, Effective field theory of dark energy: A dynamical analysis, J. Cosmol. Astropart. Phys. 02 (2014) 026.
[22] C. Armendariz-Picon, V. Mukhanov, and P. J. Steinhardt, Essentials of k-essence, Phys. Rev. D **63**, 103510 (2001).
[23] M. Malquarti, E. J. Copeland, A. R. Liddle, and M. Trodden, A new view of k-essence, Phys. Rev. D **67**, 123503 (2003).
[24] C. Armendariz-Picon and E. A. Lim, Haloes of k-essence, J. Cosmol. Astropart. Phys. 08 (2005) 007.
[25] C. Ahn, C. Kim, and E. V. Linder, Dark energy properties in dbi theory, Phys. Rev. D **80**, 123016 (2009).
[26] L. P. Chimento, R. Lazkoz, and I. Sendra, Dbi models for the unification of dark matter and dark energy, Gen. Relativ. Gravit. **42**, 1189 (2010).
[27] R.-G. Cai and S.-J. Wang, Dark matter superfluid and dbi dark energy, Phys. Rev. D **93**, 023515 (2016).
[28] S. Chattopadhyay and U. Debnath, Interaction between dbi-essence and other dark energies, Int. J. Theor. Phys. **49**, 1465 (2010).
[29] G. Calcagni and A. R. Liddle, Tachyon dark energy models: Dynamics and constraints, Phys. Rev. D **74**, 043528 (2006).
[30] J. Bagla, H. K. Jassal, and T. Padmanabhan, Cosmology with tachyon field as dark energy, Phys. Rev. D **67**, 063504 (2003).
[31] E. J. Copeland, M. R. Garousi, M. Sami, and S. Tsujikawa, What is needed of a tachyon if it is to be the dark energy?, Phys. Rev. D **71**, 043003 (2005).
[32] S. M. Micheletti, Observational constraints on holographic tachyonic dark energy in interaction with dark matter, J. Cosmol. Astropart. Phys. 05 (2010) 009.
[33] A. Sheykhi, M. Sadegh Movahed, and E. Ebrahimi, Tachyon reconstruction of ghost dark energy, Astrophys. Space Sci. **339**, 93 (2012).
[34] J. Kehayias and R. J. Scherrer, New generic evolution for k-essence dark energy with $w \approx -1$, Phys. Rev. D **100**, 023525 (2019).
[35] T. Chiba, S. Dutta, and R. J. Scherrer, Slow-roll k-essence, Phys. Rev. D **80**, 043517 (2009).
[36] R. Das, T. W. Kephart, and R. J. Scherrer, Tracking quintessence and k-essence in a general cosmological background, Phys. Rev. D **74**, 103515 (2006).
[37] S. Hannestad, Constraints on the sound speed of dark energy, Phys. Rev. D **71**, 103519 (2005).
[38] R. de Putter, D. Huterer, and E. V. Linder, Measuring the speed of dark: Detecting dark energy perturbations, Phys. Rev. D **81**, 103513 (2010).
[39] G. Ballesteros and J. Lesgourgues, Dark energy with non-adiabatic sound speed: Initial conditions and detectability, J. Cosmol. Astropart. Phys. 10 (2010) 014.
[40] M. S. Linton, A. Pourtsidou, R. Crittenden, and R. Maartens, Variable sound speed in interacting dark energy models, J. Cosmol. Astropart. Phys. 04 (2018) 043.
[41] R. Bean and O. Dore, Probing dark energy perturbations: The dark energy equation of state and speed of sound as measured by wmap, Phys. Rev. D **69**, 083503 (2004).
[42] D. J. Eisenstein, Dark energy and cosmic sound, New Astron. Rev. **49**, 360 (2005).
[43] O. Sergijenko and B. Novosyadlyj, Sound speed of scalar field dark energy: Weak effects and large uncertainties, Phys. Rev. D **91**, 083007 (2015).
[44] K. Jani, M. Abernathy, E. Berti, V. Boschi, S. Chakrabarti, A. Cocoros, J. W. Conklin, T. Creighton, S. Dell'Agnello, J.-C. Diels *et al.*, Laser interferometer lunar antenna (LILA): Advancing the us priorities in gravitational-wave and lunar science, arXiv:2508.11631.
[45] V. Mukhanov, *Physical Foundations of Cosmology* (Cambridge University Press, Cambridge, England, 2005).
[46] C.-P. Ma and E. Bertschinger, Cosmological perturbation theory in the synchronous and conformal Newtonian gauges, Astrophys. J. **455**, 7 (1995).
[47] W. Hu, Structure formation with generalized dark matter, Astrophys. J. **506**, 485 (1998).
[48] M. Tegmark, A. Taylor, and A. Heavens, Karhunen-Loeve eigenvalue problems in cosmology: How should we tackle large data sets?, Astrophys. J. **480**, 22 (1997).
[49] J. R. Bond, A. H. Jaffe, and L. Knox, Estimating the power spectrum of the cosmic microwave background, Phys. Rev. D **57**, 2117 (1998).
[50] S. Hamimeche and A. Lewis, Likelihood analysis of CMB temperature and polarization power spectra, Phys. Rev. D **77**, 103013 (2008).
[51] M. Wade, A. D. Viets, T. Chmiel, M. Stover, and L. Wade, Improving LIGO calibration accuracy by using time-dependent filters to compensate for temporal variations, Classical Quantum Gravity **40**, 035001 (2023).
[52] S. L. Larson, W. A. Hiscock, and R. W. Hellings, Sensitivity curves for spaceborne gravitational wave interferometers, Phys. Rev. D **62**, 062001 (2000).
[53] C. Cutler, Angular resolution of the LISA gravitational wave detector, Phys. Rev. D **57**, 7089 (1998).
[54] F. A. Jenet, G. B. Hobbs, K. J. Lee, and R. N. Manchester, Detecting the stochastic gravitational wave background using pulsar timing, Astrophys. J. Lett. **625**, L123 (2005).
[55] X. Siemens, J. Ellis, F. Jenet, and J. D. Romano, The stochastic background: Scaling laws and time to detection for pulsar timing arrays, Classical Quantum Gravity **30**, 224015 (2013).
[56] A. Sesana and A. Vecchio, Measuring the parameters of massive black hole binary systems with Pulsar Timing Array observations of gravitational waves, Phys. Rev. D **81**, 104008 (2010).
[57] K. N. Abazajian *et al.* (CMB-S4 Collaboration), CMB-S4 science book, first edition, arXiv:1610.02743.
[58] K. Abazajian, G. Addison, P. Adshead, Z. Ahmed, S. W. Allen, D. Alonso, M. Alvarez, A. Anderson, K. S. Arnold, C. Baccigalupi *et al.*, CMB-S4 science case, reference design, and project plan, arXiv:1907.04473.
[59] K. Abazajian *et al.* (CMB-S4 Collaboration), CMB-S4: Forecasting constraints on primordial gravitational waves, Astrophys. J. **926**, 54 (2022).

[60] A. Loeb and M. Zaldarriaga, Measuring the small—scale power spectrum of cosmic density fluctuations through 21 cm tomography prior to the epoch of structure formation, Phys. Rev. Lett. **92**, 211301 (2004).
[61] J. R. Pritchard and A. Loeb, 21-cm cosmology, Rep. Prog. Phys. **75**, 086901 (2012).
[62] N. Aghanim, T. Ghosh, J. J. Bock, B. P. Crill, O. Doré, S. R. Hildebrandt, G. Rocha, K. M. Górski, C. R. Lawrence, S. Mitra, G. Roudier, and P. Collaboration, Planck 2018 results. VI. Cosmological parameters, Astron. Astrophys. **641**, A6 (2020).